

## MONTE CARLO SIMULATION OF STEADY-STATE TRANSPORT IN SUBMICROMETER InP AND GaAs $n^+ - i(n) - n^+$ DIODE

H. ARABSHAHI\*, M. REZAEI ROKN-ABADI and F. BADIEIAN BAGHSIAHI

*Department of Physics, Ferdowsi University of Mashhad, Mashhad, Iran*

*\*arabshahi@um.ac.ir*

M. R. KHALVATI

*Department of Physics, Shahrood University of Technology, Shahrood, Iran*

Received 18 May 2009

Revised 13 October 2009

Monte Carlo simulation of electron transport in an InP diode of  $n^+ - i(n) - n^+$  structure is compared with GaAs diode. The anode voltage ranges from 0.5 to 1.5 V. The distributions of electron energies and electron velocities and the profiles of the electron density, electric field and potential and average electron velocity are computed. Based on these data, the near ballistic nature of the electron transport in the 0.2  $\mu\text{m}$ -long diode and the importance of the back-scattering of electrons from the anode  $n^+$ -layer are discussed. In addition, the effects of the lattice temperature and doping on the length of the active layer are discussed. Electronic states within the conduction band valleys at the  $\Gamma$ ,  $L$ , and  $X$  are represented by non-parabolic ellipsoidal valleys centered on important symmetry points of the Brillouin zone. Our simulation results have also shown that the electron velocity characteristics in InP diode are more sensitive to temperature than in other III-V semiconductors such as GaAs.

*Keywords:* Electric field; back-scattering; non-parabolic; Brillouin zone.

### 1. Introduction

The diode structure is one of the most favored devices in the construction of large-scale integrated circuits because of its simplicity of construction, the comparative lack of dopant diffusion problems and the resultant high-packing densities possible. Whilst the preferred semiconductor is still silicon, industry is now tooling up for GaAs production, which offers higher electron mobility and hence the prospect of greater frequency-operating rates. Its direct band gap furthermore allows easier integration with optical devices. For this reason, GaAs devices have received much attention in the literature, particularly with respect to their simulation<sup>1,2</sup> in an attempt to understand the basic principles of their operation. Monte Carlo methods

\*Corresponding author.

have been used largely in this effort because they allow an essentially exact solution of the Boltzmann transport equation and are subjected only to statistical errors, unlike drift diffusion models which cannot accurately treat the hot-electron effects that are present to a high degree in small GaAs devices.<sup>3,4</sup> Perhaps the best illustration of this is the remarkable agreement with experiment obtained by Fischetti and Laux<sup>5</sup> with a Monte Carlo MOSFET simulation, in which significant velocity overshoot was observed near the drain end of the device.

InP offers the prospect of mobilities comparable to GaAs and is increasingly being developed for the construction of optical switches. Other authors have also pointed out the potential importance of InP and a few simple devices have been simulated.<sup>6</sup> InP has unfortunately proved to be a difficult material to work with in practice and very little experimental work has been done because of technical problems in forming Schottky contacts with sufficiently high barrier potentials.<sup>7,8</sup> Nevertheless, some experimental work has been done on other types of InP field effect transistor, most notably MISFETs,<sup>9,10</sup> and there is every reason to be optimistic that some form of heterojunction under the gate may well overcome the problem of the low barrier. In this article, we show that, if the aforementioned problems can be overcome, InP shows every indication that it will fulfill its promise as a useful material. However, simulations for higher anode voltages are needed in view of the situation in practical devices where engineering problems call for anode voltages of no less than about the Schottky barrier height or the  $p$ - $n$  junction barrier height. The boundary conditions are important as they have significant influence on the space-charge-limited current flow, which becomes dominant in submicron devices. In this article, we report an ensemble Monte Carlo simulation of the electron transport in a submicron InP and GaAs diodes with highly doped  $n^+$ -layer employed as cathode and anode. The anode voltage applied to the diode ranges from 0.5 to 1.5 V. This article is organized as follows.

Details of the device fabrication and Monte Carlo model, which is used in the simulated device, are presented in Sec. 2 and results for simulations carried out on the device are interpreted in Sec. 3.

## 2. Model, Device and Simulations

An ensemble Monte Carlo simulation has been carried out to simulate the electron transport properties in InP and GaAs based  $n^+ - i(n) - n^+$  diodes. The method simulates the motion of charge carriers through the device by following the progress of  $10^4$  superparticles. These particles are propagated classically among collisions according to their velocity, effective mass and the prevailing field. The selection of the propagation time, scattering mechanism and other related quantities is achieved by generating random numbers and using these numbers to select, for example, a scattering mechanism. In order to describe all these effects accurately, it is necessary to have knowledge about the geometry and dimensions of the device, the band structure of the material used, and other physical constants that are necessary for calculating the rates for the relevant carrier scattering mechanisms.

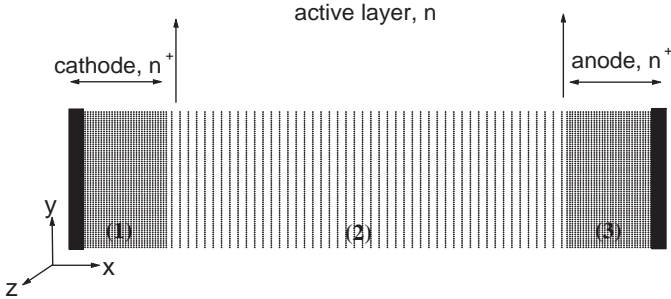


Fig. 1. Device geometry and discretization of an  $n^+ - i(n) - n^+$  diode. There are three regions. The mesh cells are uniform within any single region and match at the joints.

The geometry of the device to be simulated is specified at the beginning of the simulation by defining it in an  $x$ - $y$  plane as a set of joined rectangular regions, each with uniform doping and other material parameters, and a set of contact regions. All physical quantities are assumed constant in the  $z$ -direction (device width). Figure 1 shows a simple example of joined rectangular regions and contacts for an  $n^+ - i(n) - n^+$  diode structure. The solution of Poisson's equation is based on a finite difference method which requires that all the rectangular regions of the device are divided into uniform arrays of two-dimensional mesh cells. The cells may differ in form from region to region but it is necessary that they match in size along the joint between two adjacent regions. In Fig. 1, the rectangular regions 1 and 3 have identical uniform mesh cells which are different from those in region 2, but match at the joints. The cells also form the frame of reference in which the particles move under the influence of the electric field. The definition of the mesh (shape and size of the cells) is dependent on the details of the device and the simulation, since, for example, the resolution of the electric field is limited by the size of the mesh cells.

After setting all the material and device parameters, the simulation is started in a state of charge neutrality everywhere in the device. The simulated particles are distributed appropriately among all the mesh cells to achieve the required neutrality. Because the number of electrons in a real device ( $n$ ) is normally extremely large, it is impossible to simulate the motion of all the particles by the Monte Carlo method. Therefore, in the self-consistent approach, a set of  $N_{\text{sp}}$  superparticles ( $N_{\text{sp}} \ll n$ ), which are intended to be representative of the electrons, is considered instead. For the superparticle dynamics to be representative of the electrons, the response of each superparticle to the electric field and scattering interactions must be the same as that of an electron. However, for the purposes of calculating the electric field inside the device and the current flow through the electrodes, it is necessary for the total charge of the superparticles to be the same as the total electronic charge. In the two-dimensional device models used here, there is no variation of electron density or electric field normal to the  $x$ - $y$  plane and the superparticles may be

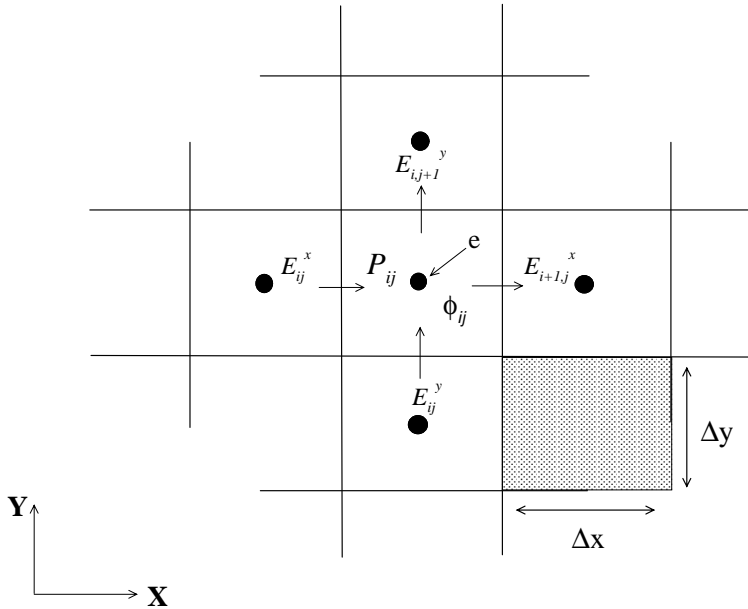


Fig. 2. The nearest-grid-point method for charge assignment in two-dimensions. The charge density at a mesh point  $P_{ij}$  is taken to be the total charge in the mesh cell surrounding the mesh point  $P_{ij}$  divided by the cell area. Note discretized electric field  $E_{ij}$  and electric potential  $\phi_{ij}$ , ( $E = -\nabla\phi$ ) are used in the solution of Poisson's equation.

considered to be charge rods extending infinitely in the  $z$ -direction. The charge per unit length of the charge rods is then taken as

$$q_{\text{sp}} = -en/N_{\text{sp}}W, \quad (1)$$

where  $W$  is the device width. It then follows that the total superparticle charge in a range of  $z$  equal to the device width is the same as the total electronic charge within the real device.

Initially, all the superparticles in the device are made to occupy the lowest conduction band valley of the constituent semiconductor and are assigned wavevectors corresponding to a Maxwellian distribution. The superparticle system is sampled at regular intervals (typically 1 femtosecond) and the charge within a cell is calculated. The simplest method for assigning charged particles to cells is the nearest-grid-point scheme in which the total charge found in a cell is assigned to the midpoint of that cell (Fig. 2). After each sampling, Poisson's equation is solved and the electric field is updated.

Poisson's equation is solved by a combined fast Fourier transform<sup>11–13</sup> and Buneman cyclic reduction<sup>14</sup> method developed by Walmsley and Abram.<sup>15</sup> This calculational scheme is integrated with a capacity matrix approach<sup>16</sup> that facilitates the use of individual rectangular regions to form more complicated structures.

The information on the state of each particle in the simulation may be used to calculate various properties of the ensemble and hence make predictions about

Table 1. Important parameters used in our simulations for GaAs and InP materials which are taken from Refs. 7, 8 and 17.

Bulk material parameters	GaAs	InP	
Density, $\rho$ (kgm <sup>-3</sup> )	5360	4810	
Longitudinal sound velocity, $v_s$ (ms <sup>-1</sup> )	5400	5130	
Low-frequency dielectric constant, $\epsilon_s$	12.9	12.61	
High-frequency dielectric constant, $\epsilon_\infty$	10.92	9.61	
Acoustic deformation potential, $D$ (eV)	5.0	5.0	
Polar optical phonon energy, $\hbar\omega_{\text{op}}$ (meV)	35.36	42.4	
Band gap, $E_g$ (meV)	1.42	1.34	
Valley-dependent parameters	$\Gamma$	$L$	$X$
Effective mass ( $m^*/m_0$ ):			
GaAs	0.063	0.292	0.471
InP	0.082	0.353	0.462
Non-parabolicity (eV <sup>-1</sup> ):			
GaAs	1.16	0.5	1.0
InP	0.61	0.9	1.0
Valley separation from valence band (eV):			
GaAs	1.42	1.743	1.867
InP	1.34	2.172	2.832
Number of equivalent valley	1.0	4.0	3.0

the behavior of a real material or device. For example, ensemble averages of particle velocity or energy may be obtained at a specified time, either for the whole system, or for some limited region of space. In the case of a device simulation, the currents at various terminals may also be calculated, in addition to the extraction of microscopic information.

Our self-consistent Monte Carlo simulation was also performed using an analytical band structure model consisting of three non-parabolic ellipsoidal valleys. The scattering mechanisms considered in the model are acoustic, polar optical, ionized impurity, piezoelectric, and non-equivalent intervalley scattering. The non-equivalent intervalley scattering is present among the  $\Gamma$ ,  $L$ , and  $X$  valleys. Acoustic and piezoelectric scatterings are assumed elastic and the absorption and emission rates are combined under the equipartition approximation, which is valid for lattice temperatures above 77 K. Elastic ionized impurity scattering is described using the screened Coulomb potential of the Brooks–Herring model. Steady-state results of high-field transport studies have been obtained for lattice temperatures up to 450 K, to gain some insight into the hot carrier transport and the energy distribution function that would be generated in the gate-drain region of a power-field effect transistor. The parameters used in the present Monte Carlo simulation are the same as those used by Arabshahi *et al.*<sup>17</sup> for bulk simulation in InP and GaAs materials and are listed in Table 1.

The diode geometry used in all the simulations had a overall length of  $0.5 \mu\text{m}$  in the  $x$ -direction. A lightly doped active layer ( $n$ -layer) is sandwiched between cathode and anode layers, which are abruptly doped with a donor density of  $10^{24} \text{m}^{-3}$ . The length of the active layer is  $0.2 \mu\text{m}$ . Approximately  $10^4$  superparticles are used in the simulation and lattice temperatures up to 450 K are considered. The applied anode voltage is varied between 0.5 and 1.5 V to investigate the effects of field variations on the transport properties. This range of voltages is large enough that velocity overshoot and intervalley transfer effects occur.

### 3. Simulation Results

In this article, we report the use of the ensemble Monte Carlo simulation to study the properties of InP and GaAs  $n^+-i(n)-n^+$  diodes. The motivation for the study is that the simulation of the simple structure can provide useful insight into some of the transport effects that occur in the more complex devices such as MESFETs and HFETs. Tomizama *et al.*<sup>18</sup> were the first to simulate a submicron GaAs  $n^+-i(n)-n^+$  diode by the ensemble Monte Carlo technique using just a two-valley model. Our simulations are similar in nature but use the three-valley model appropriately for zinc blende InP and GaAs. Steady-state results of high-field transport studies have been obtained for lattice temperatures up to 450 K, to gain some insight into the hot carrier transport and the energy distribution function that would be generated in the gate-drain region of a power-field effect transistor.

Figure 3 shows the distribution of hot electrons throughout the GaAs and InP  $n^+-i(n)-n^+$  diodes in the steady state at 300 K with a bias of 1.5 V when the active layer doping level is  $10^{21} \text{m}^{-3}$ . It is apparent that there is significant concentration in the satellite valleys on the anode side of the active layer (higher velocity points). These electrons have attained enough energy under the action of the electric field to be scattered into satellite valleys.

Figures 3(a) and 3(b) show the corresponding distribution of velocity and energy parallel to the electric field. The electrons in the active layer can be divided into three main categories:

1. Electrons in the  $\Gamma$  valley, traveling more or less ballistically toward the anode.
2. Electrons in the satellite valleys, which have been excited by the field in the active layer.
3. Electrons in the  $\Gamma$  valley, which have been back-scattered from the anode  $n^+$ -layer.

The electric field in the device as a function of position is shown in Fig. 4 for anode voltages between 0.5 and 1.5 V. It is apparent from this figure that essentially all the potential is dropped in the active layer. However, because of the inhomogeneous space charge the field does vary substantially with position, reaching a maximum magnitude near the anode. The high value of the field near the anode is responsible for the almost ballistic acceleration of the electrons as soon as they enter the active

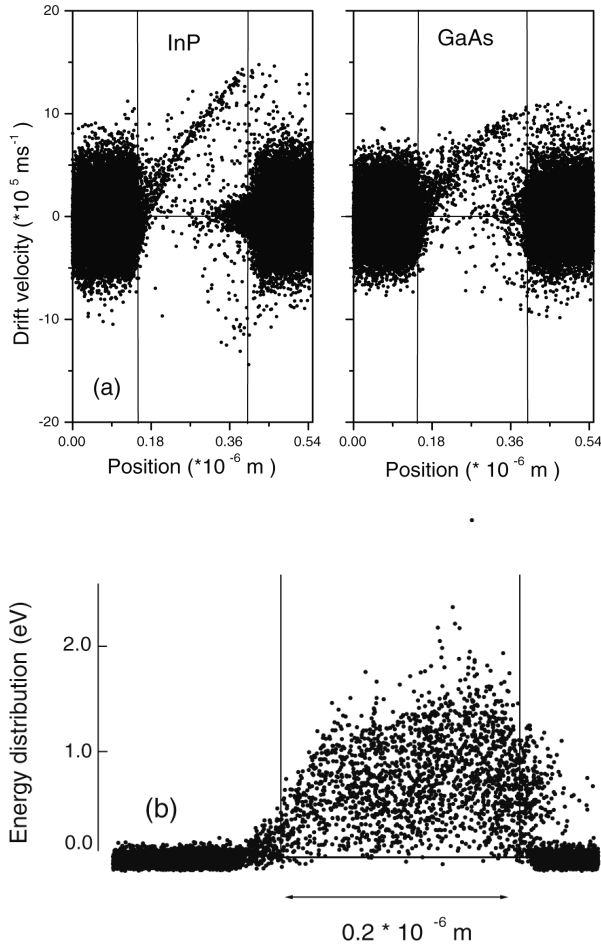


Fig. 3. Hot electron position throughout the simulated GaAs and InP  $n^+ - i(n) - n^+$  diodes, (a) velocity distribution and (b) energy distribution. The higher velocity points represent hot electrons in the upper valleys ( $L$  and  $X$  valleys). The applied anode voltage is  $V_a = 1.5 \text{ V}$  and the results are at room temperature.

region. Comparison of electric field variation in GaAs and InP diodes show that GaAs-based devices should have higher output drain current and velocity overshoot effects.

Figures 5 and 6 show some features of the state of the InP diode in comparison with GaAs diode at temperature of 300–450 K when the applied voltage is 0.5 or 1.5 V. The free electron concentration through the device is plotted in Fig. 5(a). The electrons diffuse from the cathode and anode into the active layer and are accelerated toward the anode by the field. The resulting space charge causes the departure from a uniform electric field, which is clearly apparent in Fig. 4.

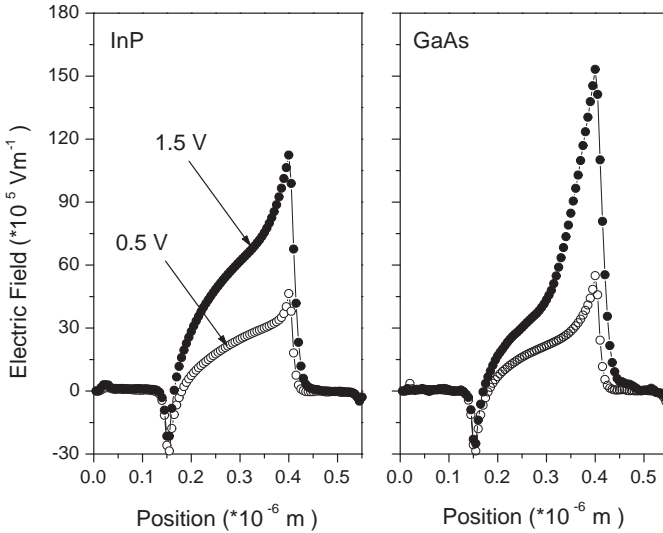


Fig. 4. The electric field in the GaAs and InP  $n^+ - i(n) - n^+$  diodes for anode voltages between 0.5 and 1.5 V at room temperature.

Figure 5(b) shows that the average drift velocity in the active layer has a maximum value of about  $4.7 \times 10^5 \text{ ms}^{-1}$  in InP diode and  $4.4 \times 10^5 \text{ ms}^{-1}$  in GaAs diode at 300 K. Raising the temperature to 450 K reduces the maximum drift velocity to a value of  $4 \times 10^5 \text{ ms}^{-1}$  in the case of InP diode. This shows InP characteristics are superior to GaAs. Therefore, the InP devices displayed substantially greater stability with respect to changes of voltage and temperature because of the ability of InP to maintain a positive differential resistance at the drain contact due to ballistic effects under the gate.

A similar decrease of drift velocity with temperature is seen in bulk material and is due to increased electron scattering.

The plot of average electron kinetic energy across the device (Fig. 6(a)) provides further information on the dynamics. The electrons reach an average energy of 0.18 eV near the anode region and the more energetic electrons in the distribution have sufficient energy to transfer to the upper valleys. Finally, the  $\Gamma$  valley energy profile for two different temperatures is illustrated in Fig. 6(b).

As it can be seen from Figs. 5 and 6 that increasing the temperature from 300 to 450 K causes some decrease in the electron transport characteristics of simulated diodes. As noted earlier, this effect is due to increased phonon scattering, which suppresses the heating of carriers by the electric field. Note, however, the effect is relatively small when considering the large increase in temperature.

To investigate the temperature dependence of the valley occupancy in the active layer, we have simulated the GaAs and InP  $n^+ - i(n) - n^+$  diodes with an applied voltage of 1.5 V and temperatures of 300–450 K. The results are presented in Fig. 7. The high electric field in the active layer creates a significant electron population



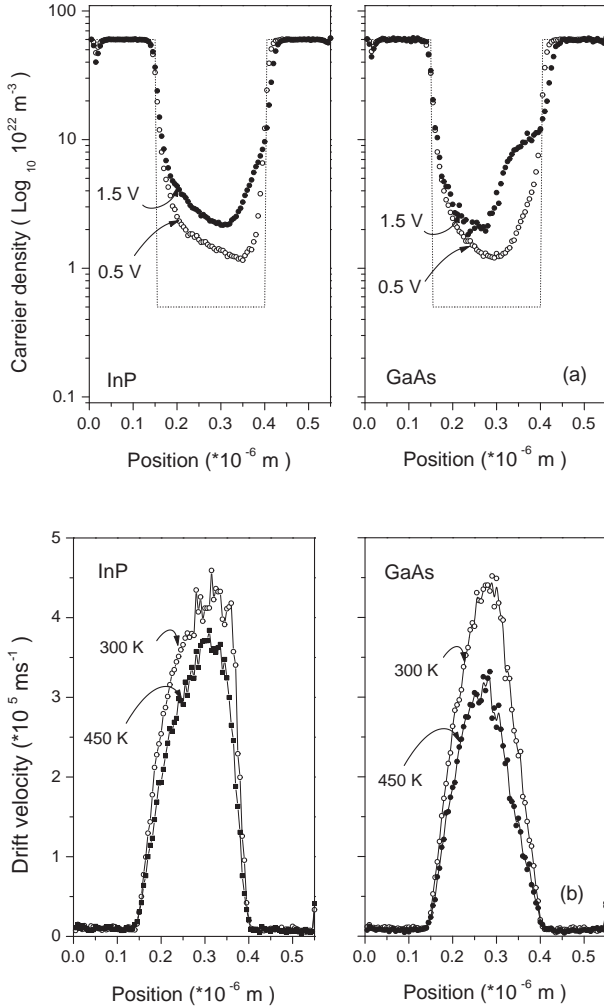


Fig. 5. Electron transport characteristics as a function of position in the model GaAs and InP diodes at different temperatures. (a) Electron concentration and (b) average drift velocity for  $V_a = 1.5 \text{ V}$ .

in the  $L$  and  $X$  valleys. Increasing the temperature from 300 to 450 K causes some increase in the population of the higher valleys due to increasing intervalley scattering rate.

#### 4. Conclusion

In this article, the results of simulations of electron transport in GaAs and InP  $n^+ - i(n) - n^+$  diodes have been reported. The diodes have highly doped  $n^+$ -layers serving as the cathode and anode. The anode voltages  $V_a$  ranged from 0.5 to 1.5 V and lattice temperatures between 300 and 450 K have been considered. The electrons

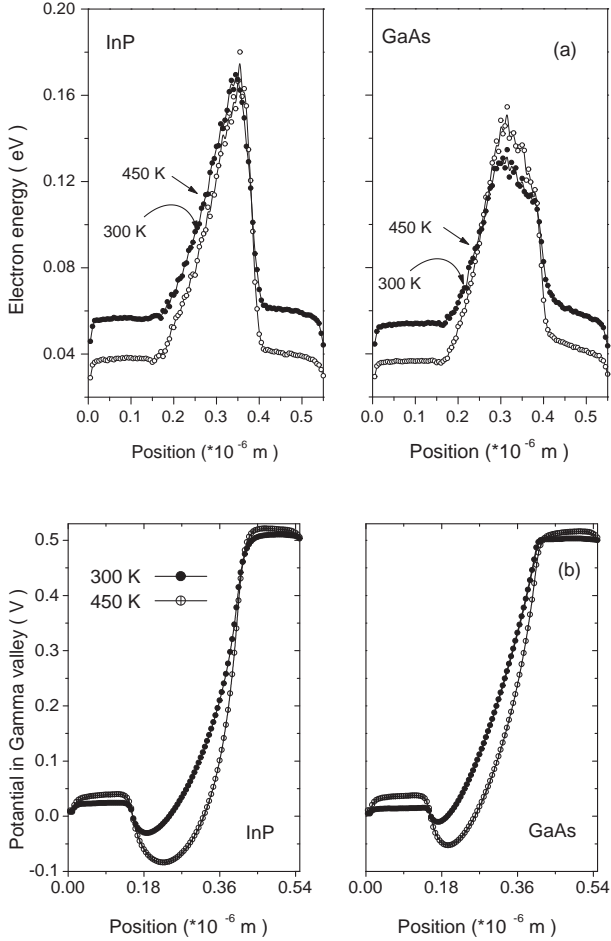


Fig. 6. Electron transport characteristics as a function of position in the model GaAs and InP diodes at different temperatures. (a) Average kinetic energy and (b)  $\Gamma$  valley energy profile for  $V_a = 1.5$  V.

injected from the cathode initially travel quasi-ballistically but there is substantial transfer to the upper satellite valleys as the anode is approached, resulting in a reduced average electron velocity in that region. The peak drift velocity ranges from about  $4 \times 10^5$   $\text{ms}^{-1}$  to  $4.7 \times 10^5$   $\text{ms}^{-1}$ , with a donor density of  $10^{21}$   $\text{m}^{-3}$  and an active layer length of  $0.2 \mu\text{m}$  for both GaAs and InP semiconductors. Raising the lattice temperature to 450 K reduces the peak drift velocity, but it still remains above  $3.5 \times 10^5$   $\text{ms}^{-1}$ . Our results also show that InP devices have better performance than GaAs ones.

### Acknowledgment

We would like to thank M. G. Paezi for the partial support of this work.

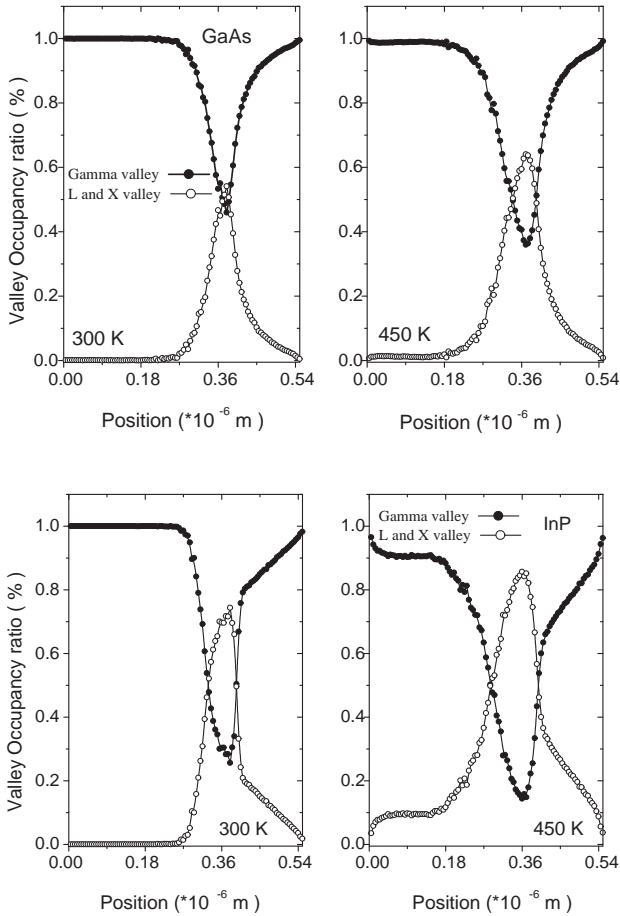


Fig. 7. Fractional occupation of the central  $\Gamma$ ,  $L$ , and  $X$  valleys in GaAs and InP  $n^+ - i(n) - n^+$  diodes as a function of position.

## References

1. R. A. Warniear, *Solid State Electron Devices* **1** (1977) 97.
2. A. Yoshii, M. Tomizawa and K. Yokoyama, *IEEE Trans. Electron Devices* **30** (1983) 1376.
3. G. Baccarani, C. Jacoboni and A. Mazzone, *Solid State Electron* **20** (1977) 5.
4. D. C. Herbert, *Semicond. Sci. Technol.* **6** (1991) 405.
5. M. V. Fischetti and S. E. Laux, *Phys. Rev. B* **38** (1988) 9721.
6. K. Brennan, K. Hess and J. Tang, *IEEE Trans. Electron Devices* **30** (1983) 1750.
7. N. Newman, T. Kendelewicz and W. Spicer, *Appl. Phys. Lett.* **46** (1985) 1176.
8. N. Newman, M. Schilfgaarde and T. Kendelewicz, *Mater. Res. Soc. Symp. Proc.* **54** (1986) 433.
9. D. C. Cameron, L. D. Irving and J. Woodward, *Thin Solid Films* **103** (1983) 61.
10. D. C. Cameron, L. D. Irving and L. D. Whitehouse, *Electron Lett.* **18** (1982) 534.
11. J. W. Cooley and J. W. Tukey, *Math. Comput.* **19** (1965) 297.

12. G. B. Bergland, *Math. Comput.* **21** (1967) 236.
13. G. B. Bergland, *Math. Comput.* **22** (1968) 275.
14. C. Temperton, *J. Comput. Phys.* **34** (1980) 314.
15. M. Walmsley and R. A. Abram, *Int. J. Comput. Math.* **15** (1996) 31.
16. B. L. Buzbee, *SIAM J. Numer. Anal.* **18** (1971) 722.
17. H. Arabshahi, M. R. Khalvati and M. R. Rokn-Abadi, *Mod. Phys. Lett. B* **22** (2008) 1695.
18. K. Tomizawa, Y. Awano and N. Hashizume, *IEE Proc.* **129** (1982) 131.